Available online at www.sciencedirect.com
SCIENCE DIRECT®
Journal of Sound and Vibration 278 (2004) 135–153
JOURNAL OF SOUND AND VIBRATION
www.elsevier.com/locate/jsvi

The energy source simulation method

D.W. Herrin*, T.W. Wu, A.F. Seybert

Department of Mechanical Engineering, University of Kentucky, 521 CRMS Building, Lexington, KY 40506-0108, USA

Received 3 August 2001; accepted 1 October 2003

Abstract

An energy source simulation method (ESSM) has been developed to determine sound energy density. Using this approach, a specified intensity boundary condition on the surface of a vibrating body is approximated by superimposing energy density sources located outside the acoustic domain. The unknown strengths for these sources are then found by minimizing the error on the boundary, using a least-squares technique. The superposition of these energy density sources should then approximate the sound radiating from the body. The approach was evaluated for radiation problems in two-dimensions for circular and square boundaries. The ESSM proved an excellent tool for predicting the energy density provided that power radiated uniformly along the boundary. However, the ESSM could not accurately predict the directivity characteristics of the energy density field if the power radiated significantly higher from one side of an object than other sides. The ESSM was also applied to both an interior and exterior scattering problem with similar results.

1. Introduction

Over the past several years, numerical methods have been increasingly used to predict vibration and noise. These methods enable engineers to investigate the impact that design changes have on the acoustics prior to the development of costly prototypes. Today, deterministic methods like the finite and boundary element methods have been integrated into the product development cycles in many industries. However, these deterministic methods are problematic at high frequencies due to typical geometric and material variability, and the number of nodes required for high frequency problems. Consequently, energy based methods are being increasingly used as an alternative to the deterministic methods. Statistical energy analysis (SEA), the most widely used and accepted of these methods, is a lumped parameter method where a system, assumed to have sufficient modal

*Corresponding author. Fax: +1-859-257-3304.
E-mail address: dwherr01@engr.uky.edu (D.W. Herrin).

0022-460X/$ - see front matter
doi:10.1016/j.jsv.2003.10.019

density, is treated in a statistical sense, and the dissipated power is assumed to be proportional to the energy density in a subsystem [1,2]. Energy is then assumed to flow from subsystems having higher modal energies to those with lower modal energies. However, SEA cannot easily predict the spatial variation of energy within subsystems and the effect of localized damping treatments.

Consequently, several authors have advocated using alternative energy flow methodologies to remedy these problems [3–10]. Most of these methods extend SEA by using a diffusion type equation to predict the energy flow. Instead of using a lumped parameter approach to predict the average energy for a subsystem, they calculate the spatial variation of energy within the subsystem allowing the analyst to predict the effects of localized damping treatments or adding ribs. These energy flow methods have even been coupled to traditional displacement based finite element methodologies to predict the acoustics for problems in the so-called "mid-frequency range" [11].

The energy methods cited above differ from each other in the differential equations that they are based on, though most of these equations are similar in form. As one would expect, some of these methods are more amenable to developing numerical solutions than others. Unfortunately, those that are assume that the solution can be accurately described by a superposition of plane waves [3–6,12]. As a result, the methods, which assume a superposition of plane waves, cannot reliably model solutions involving point sources and may be inadequate for many radiation problems [13,14]. Certainly, these methods will not perform well in the far field where a radiating body can be approximated as a point source.

The current effort reported in this paper is an attempt to alleviate the difficulties by using an energy source simulation method (ESSM). Using this technique, the intensity along the boundary is approximated by superimposing energy sources placed outside the acoustic domain. The strengths for each of the sources are found using a least-squares technique. The energy density in the acoustic domain is then found by superimposing the sources. Thus, the basic premise is that the energy density in the acoustic domain can be accurately simulated by a set of sources if the sources are placed strategically and have source strengths producing the desired boundary intensity. This paper will review the development of the ESSM and detail a few two-dimensional examples illustrating the method.

2. The energy source simulation method

The development of the ESSM [15] will be summarized in this section. Ochmann [16], and Fahnline and Koopman [17] used a similar technique for solving acoustic radiation problems with good results. They placed pressure sources on the interior of the radiating body and then optimized the source strengths to best approximate the prescribed normal velocity on the surface. In this discussion, a similar approach will be used where energy density sources will be used (instead of pressure sources) in an effort to produce the prescribed boundary intensity (instead of normal velocity). The development presented here is similar to Ochmann's [16] development for pressure sources.

It should be added that Le Bot [9] and Bitsie [18] developed similar approaches to the ESSM. Both researchers developed indirect boundary element codes and placed energy density sources on the boundary. However, there are some differences between those methods and the ESSM. Using the ESSM, the analyst can specify fewer sources than the number of elements along the boundary.

Thus, it is anticipated that the ESSM would be faster than the aforementioned boundary element approaches. However, a disadvantage of the ESSM is that the analyst will be forced to carefully place these sources within the boundary.

Fig. 1 is a schematic illustrating this concept for a radiation problem with sources located on the interior of the boundary. As shown in the figure, the normal to the boundary is given as $\hat{n}$, and the direction of the intensity from energy source i is $\hat{s}_i$. In this development, the energy density at any point is expressed as a superposition of energy sources assuming that interference effects between propagative waves can be neglected [9,14,18,19]. Le Bot [9] discussed the assumptions associated with energy methods, and the reader is encouraged to refer to that paper for more information. Each of the sources can be expressed as the product of a source strength, a_i, and a function, $G(r_i)$, proportional to the energy density. Thus, the energy density of a single source, $e(r_i)$, can be expressed as

$$e(r_i) = a_i G(r_i), \tag{1}$$

and the energy density (E) at any point in space can be written as a superposition of the N_1 virtual sources and N_2 given sources as

$$E = \sum_{i=1}^{N_1} a_i G(r_i) + \sum_{j=1}^{N_2} q_j G(r_j). \tag{2}$$

For cylindrical waves, the function proportional to the energy density is

$$G(r_i) = \frac{\mathrm{e}^{-\eta k_0 r_i}}{r_i}, \tag{3}$$

where r_i is the distance from the source, k_0 is the wave number, and η is the loss factor [14].

In a similar manner, the intensity at a point can also be expressed by superimposing the intensities associated with individual energy density sources. It is helpful to relate the intensity to the energy density for a single source using an expression commonly used for propagating phenomenon,

$$\vec{i}(r_i) = c_g e(r_i)\hat{s}_i = a_i c_g G(r_i)\hat{s}_i, \tag{4}$$

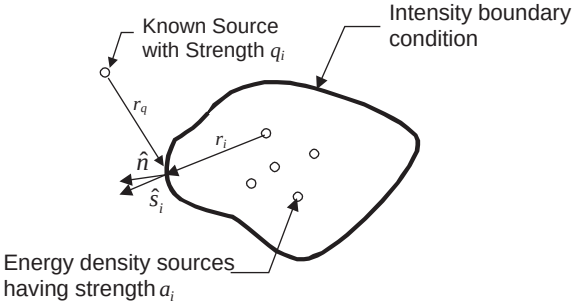

Fig. 1. Schematic showing energy density sources inside boundary. Energy density sources are indicated by ○.

where c_g is the group speed [19]. Then, the intensity at any point in space can be expressed as

$$\vec{I} = \sum_{i=1}^{N_1} a_i c_g G(r_i)\hat{s}_i + \sum_{j=1}^{N_2} q_i c_g G(r_j)\hat{s}_j. \tag{5}$$

The normal intensity at the boundary can be found by taking the dot product of the total intensity, $\vec{I}$, and the normal vector, $\hat{n}$. Then, the normal intensity at the boundary can be expressed as

$$I_n = \sum_{i=1}^{N_1} a_i c_g G(r_i)\hat{s}_i \cdot \hat{n} + \sum_{j=1}^{N_2} q_j c_g G(r_j)\hat{s}_j \cdot \hat{n} \tag{6}$$

by adding the normal components of the partial intensities (Eq. (4)).

A quadratic error function for the normal intensity at the boundary can then be defined as

$$F(a_i) = \left(I_n^{(B)} - I_n\right)^2 = \left(I_n^{(B)} - \sum_{i=1}^{N_1} a_i c_g G(r_i)\hat{s}_i \cdot \hat{n} - \sum_{j=1}^{N_2} q_j c_g G(r_j)\hat{s}_j \cdot \hat{n}\right)^2, \tag{7}$$

where $I_n^{(B)}$ is the prescribed normal intensity at the boundary. Integrating Eq. (7) around the boundary, an error functional can be written as

$$\bar{F}(a) = \int_\Gamma \left(I_n^{(B)} - \sum_{i=1}^{N_1} a_i c_g G(r_i)\hat{s}_i \cdot \hat{n} - \sum_{j=1}^{N_2} q_j c_g G(r_j)\hat{s}_j \cdot \hat{n}\right)^2 \mathrm{d}\Gamma \tag{8}$$

for a two-dimensional boundary Γ. This functional can then be minimized by taking the partial derivative with respect to each source strength and setting it equal to zero, obtaining

$$\begin{aligned}\frac{\partial \bar{F}}{\partial a_k} &= \int_\Gamma c_g G(r_k)\hat{s}_k \cdot \hat{n}\left(I_n^{(B)} - \sum_{i=1}^{N_1} a_i c_g G(r)\hat{s}_i \cdot \hat{n} - \sum_{j=1}^{N_2} q_j c_g G(r_j)\hat{s}_j \cdot \hat{n}\right)\mathrm{d}\Gamma \\ &= 0, \quad k = 1, \ldots, N_1.\end{aligned} \tag{9}$$

Eq. (9) can be rewritten as

$$\begin{aligned}&\int_\Gamma c_g G(r_k)\hat{s}_k \cdot \hat{n}\left(\sum_{i=1}^{N_1} a_i c_g G(r_i)\hat{s}_i \cdot \hat{n}\right)\mathrm{d}\Gamma \\ &\quad = \int_\Gamma c_g G(r_k)\hat{s}_k \cdot \hat{n}\left(I_n^{(B)} - \sum_{j=1}^{N_2} q_j c_g G(r_j)\hat{s}_j \cdot \hat{n}\right)\mathrm{d}\Gamma, \quad k = 1, \ldots, N_1.\end{aligned} \tag{10}$$

Thus, there are N_1 equations, which can be solved for the N_1 unknown source strengths. It follows that the system of equations may be written in matrix form as

$$[B]_{N_1 \times N_1}\{a\}_{N_1 \times 1} = \{C\}_{N_1 \times 1}. \tag{11}$$

The boundary can be discretized and standard Lagrangian interpolation schemes and numerical integration techniques can be used to determine the unknown source strengths. The sources may be placed at any location except at the boundary nodes, since the source function for a cylindrical

or spherical wave is singular when $r_i = 0$. The method was evaluated for several two-dimensional radiation examples. These results will be summarized in the discussion that follows.

3. Test case 1—circular boundary

Radiation from a circular boundary was investigated first, and the energy density results were compared to the closed form solution. The cylinder is the most basic test case for validating the ESSM, since the energy density in the field can be simulated by a single energy density source at the center of the cylinder for any circumferential mode of vibration.

The solution to the wave equation for the pulsating cylinder is

$$p(r) = AH_m^{(2)}(kr)\cos(m\theta), \tag{12}$$

where A is the pressure amplitude, m is the mode number, and $H_m^{(2)}$ is a Hankel function of order m [19]. The particle velocity is related to the pressure using Euler's equation

$$\vec{v}(r) = \frac{\mathrm{j}}{\rho\omega}\vec{\nabla}p(r), \tag{13}$$

where ρ is the density of the fluid and ω is the radial frequency. Then, the time averaged sound energy density and the active intensity can be expressed in terms of the sound pressure and particle velocity as

$$E = \tfrac{1}{4}\left(\rho\vec{v}\cdot\vec{v}^* + \frac{1}{\rho c_g^2}pp^*\right). \tag{14}$$

The closed form energy density was determined using this equation.

Results were first examined for the pulsating cylinder ($m = 0$) at a frequency of 1000 Hz. For this example, the radius (R) of the circle was specified to 1 m (see Fig. 2). The circular boundary was discretized using 36 equal length elements, and linear interpolation was used for these elements. The fluid medium was assumed to be air so a group speed of 343 m/s, and a density of 1.2 kg/m^3 were specified. Additionally, a small loss factor of 0.001 was assumed. The intensity boundary condition used for the ESSM was determined exactly using the closed form solution.

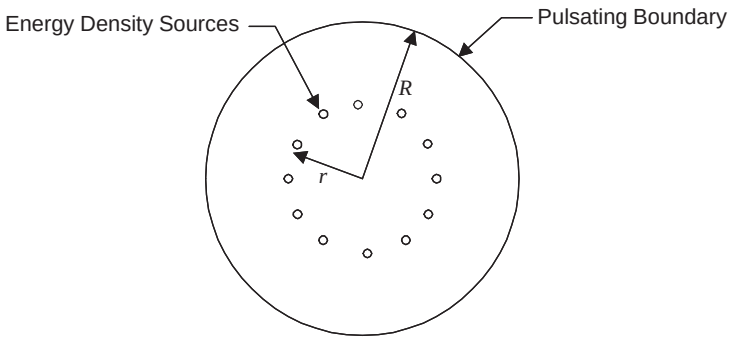

Fig. 2. Schematic showing energy density sources arranged in a circle. Energy density sources are indicated by ○.

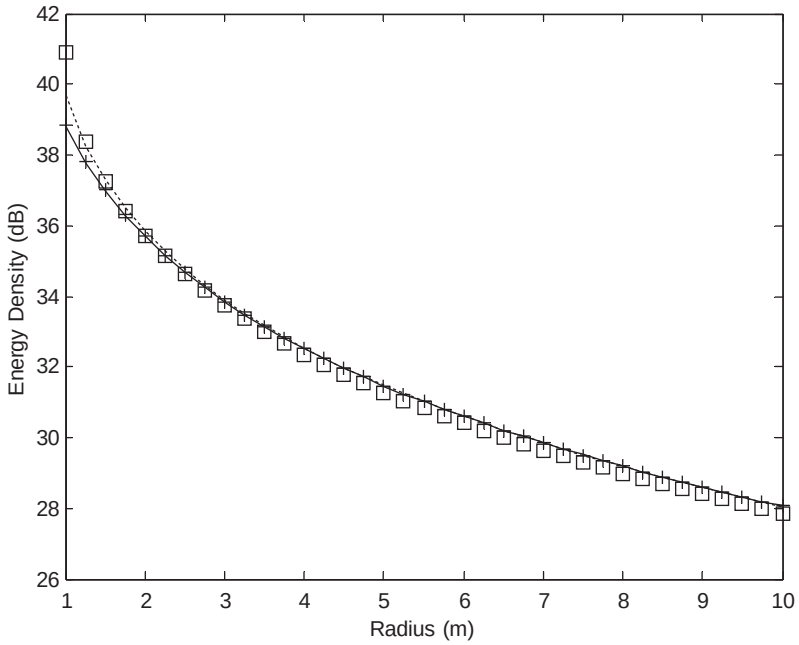

Fig. 3. Energy density comparisons (dB) for different source configurations. The reference value for the energy density is 1.0e−12 J/m^3 (—, exact energy density; + + +, 0.25 m source radius; - - - - 0.75 m source radius; □ □ □, 0.95 m source radius).

Twelve sources were placed in a circular pattern with a radius r as shown in Fig. 2. The effect of varying the radius of this pattern was investigated, and radii (r) of 0.25, 0.75, and 0.95 m were considered. As the figure indicates, the sources were spaced 30° apart about the center of the cylinder. Then the effect of varying the radius (r) on the accuracy of the ESSM was evaluated.

Fig. 3 shows a comparison of the ESSM and exact energy densities from the closed form solution for the pulsating cylinder. The energy density is plotted versus the distance from the center of the cylinder. As the figure indicates, the results compared favorably for each source configuration. Since, the closed form energy density solution is identical to that for an outgoing pressure wave centered at the center of the circle ($r = 0$ m), it was expected that smaller radii would produce the best results. However, even for the 0.95 m radius source arrangement, the energy densities compared well. The errors of largest magnitude were located close to the boundary (approximately 3 dB error).

A second analysis was also carried out using the circular geometry. This time the radius was 0.5 m and the perimeter was discretized using 72 boundary elements assuming linear interpolation. The fluid medium was assumed to have a group speed of 343 m/s, and a density of 1.2 kg/m^3 was assumed. Once again, a small loss factor of 0.001 was adopted.

For this example, the ESSM results were compared to boundary element results over a range of frequencies. The energy densities from the boundary element analysis were then summed on an octave-band basis. In order to generate the velocity boundary conditions for the subsequent boundary element analysis, a structural finite element analysis was conducted for an infinite

cylinder first. The cylinder was assumed to be 1.0 m in diameter and 0.01 m thick, and the material properties were consistent with those of steel. A broadband excitation force of 1 N was applied normal to the cylinder at a single point (Fig. 4), and the velocity was computed. The computed velocity was used as a boundary condition for subsequent boundary element analyses. Finite and boundary element analyses were conducted in the frequency range 2800–5650 Hz in steps of 50 Hz which roughly corresponds to the 4000 Hz octave band. This frequency range was selected since it

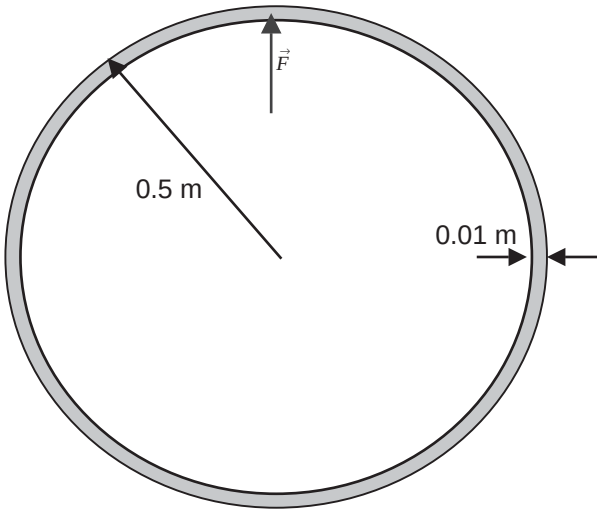

Fig. 4. Schematic showing the geometry and force location for the finite element model of the cylinder.

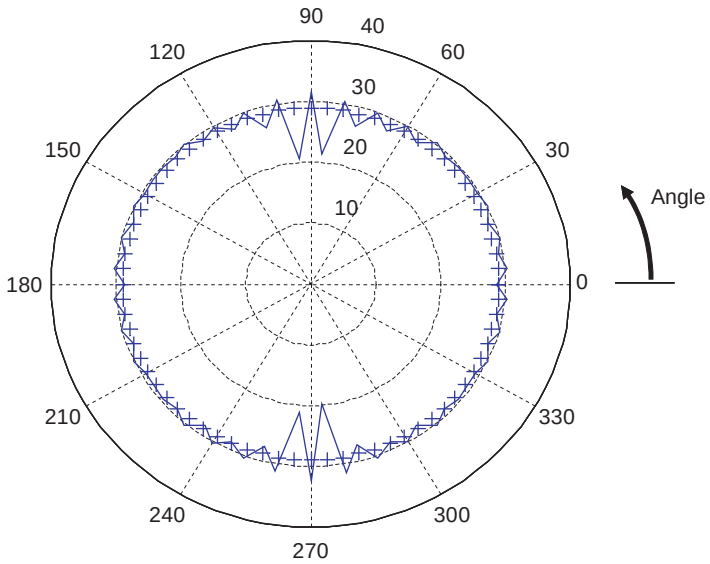

Fig. 5. Energy density comparison (dB) for the 4000 Hz octave band. The reference value for the energy density is 1.0e–12 J/m^3 (—, BEM energy density; + + +, ESSM energy density).

was sufficiently high so that the acoustic wavelength is small, and there were 20 structural modes for the cylinder in this band. The energy densities obtained from the boundary element analysis were added up over the frequency range.

In order to generate boundary conditions for the analogous ESSM analysis, the normal intensity from the BEM results was summed over the frequency range. Since the intensity pattern was roughly consistent around the circumference of the cylinder, the total intensity was simply averaged around the circumference. This average intensity was used as a boundary condition for the ESSM. The ESSM solution was then computed at the center octave band frequency (4000 Hz) for comparison sake. Twelve energy density sources were placed in a circular pattern like that shown in Fig. 2 and that pattern had a radius (r) of 0.375 m and the circular boundary had a radius (R) of 0.5 m.

The result for the 4000 Hz octave band is shown in Fig. 5. As the figure indicates, the ESSM provides an excellent prediction of the average energy density around the circumference of the field point circle. Not surprisingly though, the ESSM was unable to predict the peaks and valleys in the directivity plot because the method neglects interference effects. The average energy density around the circle was 29.1 dB using the BEM method and was 29.0 dB using the ESSM.

4. Test case 2—square boundary

Radiation from a two-dimensional $1 \times 1\,\mathrm{m}^2$ was also considered (Fig. 6). Though the two-dimensional square seems to be a simple test case, the radiated energy is very directional in nature

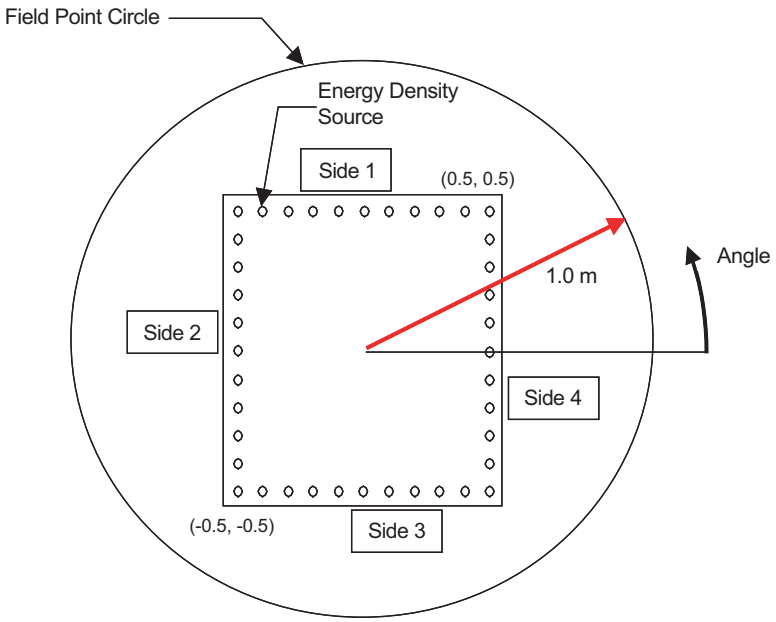

Fig. 6. Schematic showing square boundary and energy density source configuration (Configuration A). The field point circle is also indicated in the figure.

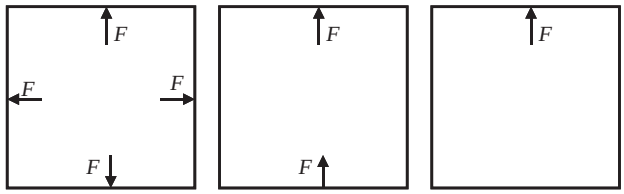

Fig. 7. Different boundary condition cases for the boundary element analyses. (a) Case A is for all sides excited, (b) Case B is for two sides excited out of phase, and (c) Case C is for only one side excited.

and far more complex than for a cylinder. In order to generate the velocity boundary conditions for the finite element analysis, a planar finite element (cross-sectional) analysis was conducted assuming a square tube cross-section. The tube was assumed to be 0.01 m thick and to have material properties consistent with steel. Three sets of forcing conditions were considered (shown in Fig. 7): all four sides excited by a force of 1 N in phase (Case A), opposite sides of the square excited out of phase with one another (Case B), and only one side excited (Case C). Additionally, closed form solutions were not so easily obtained for the acoustics, so results were again compared with two-dimensional boundary element solutions. Analyses were conducted from 2800 to 5650 Hz in 50 Hz increments. Again, this frequency range roughly corresponded to the 4000 Hz octave band, and there were 24 structural modes for the square tube cross-section in this band.

ESSM analyses were then conducted for each set of boundary conditions at a frequency of 4000 Hz. In order to specify intensity boundary conditions for the ESSM analyses, the intensity results from the BEM analyses were summed over the frequency range and averaged for each side. Since the intensity distribution was roughly consistent in amplitude along each side of the square, it was judged that the average intensity for each side would be an appropriate boundary condition.

The boundary element energy densities were calculated for the 4000 Hz octave band, and were compared to ESSM energy densities. For the ESSM analysis, the boundary was discretized into 80 equal length elements. Several source configurations were tested, and similar results were obtained for each case. The source configuration chosen for the results presented in this discussion is the one shown in Fig. 6. ESSM results were compared to boundary element results for the field point circle indicated by the figure.

Fig. 8 shows the energy density comparison for the 4000 Hz octave band for boundary condition Case A. The average energy density around the circumference of the circle was 27.9 dB using the BEM and was 28.4 dB using the ESSM. For this geometry and excitation, the energy density was more directional with the highest energy density predictably along the center of each side. In contrast, the ESSM results did not predict the variations in the energy density, but tended to smooth the energy density equally around the circle. However, the ESSM still provided a reasonable gage of the mean energy density over the region.

Fig. 9 shows the results for boundary condition Case B with the two opposite sides excited out of phase. These results are very similar to those just presented. Once again, the ESSM over predicted the energy density on average and under-predicted the peaks in the energy density at the center of each side of the square by about 6 dB. The average BEM energy density was 31.2 dB

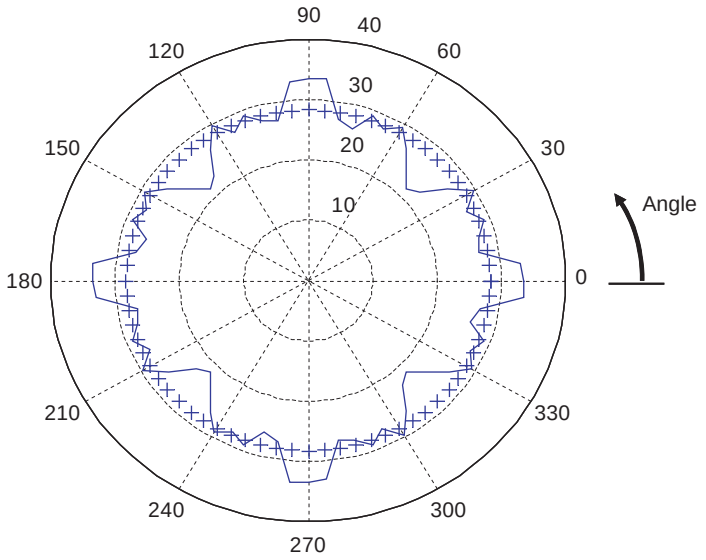

Fig. 8. ESSM energy density results for boundary condition Case A. The reference value for the energy density is 1.0e–12 J/m^3 (—, BEM energy density; + + +, ESSM energy density).

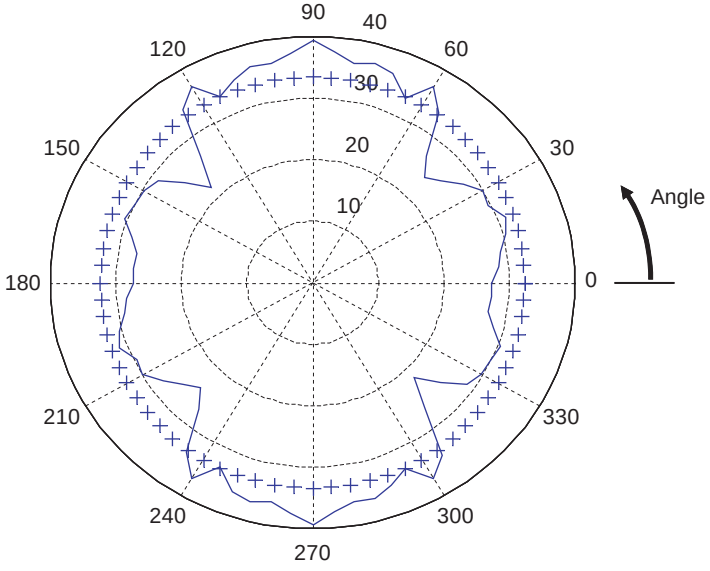

Fig. 9. ESSM energy density results for boundary condition Case B. The reference value for the energy density is 1.0e–12 J/m^3 (—, BEM energy density; + + +, ESSM energy density).

compared with 32.9 dB predicted using the ESSM. However, the ESSM over predicted the energy in the center of the two sides that were not excited (sides 2 and 4) by approximately 2 dB.

Fig. 10 shows the results for boundary condition Case C with only one side excited by the force. For this case, the average ESSM energy density was 32.7 dB, which compared reasonably well

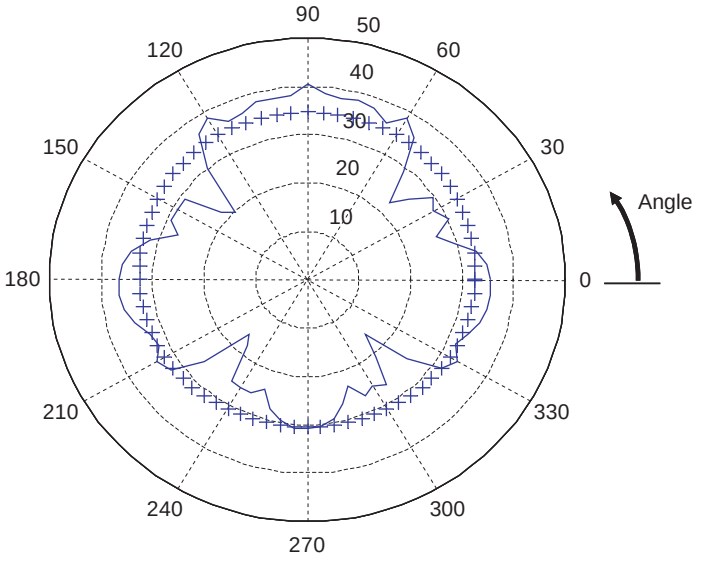

Fig. 10. ESSM energy density results for boundary condition Case C. The reference value for the energy density is 1.0e–12 J/m^3 (—, BEM energy density; + + +, ESSM energy density).

with the average BEM energy density of 30.9 dB. Once again, the ESSM tend to smooth the energy distribution around the circumference under-predicting the peak energy density while over-predicting the energy density on the side opposite to the force, and in the portions of the circle nearest to the corners.

A final case was conducted on the square geometry with Side 1 (indicated in Fig. 7) vibrating as a piston with a velocity of 1.00e–4 m/s. This test case was selected to highlight the limitations of the ESSM. The normal intensity on the boundary was determined using the equation [17]

$$I_n = \tfrac{1}{2}\rho c_g v^2, \tag{15}$$

where v is the average amplitude of the normal velocity of a side which in this case was 1.00e–4 m/s. A subsequent boundary element analysis confirmed that the intensity given by Eq. (15) was nearly correct. Additionally, the intensity was assumed to be uniform across the side, so that a constant normal intensity could be used at each point on a side for the ESSM.

The ESSM results did not compare as closely to the BEM results for this boundary condition case. As Fig. 11 indicates, the energy density compared best in the region in close proximity to the vibrating side. However, in the region opposite to the pulsating side, the ESSM over-predicted the energy density by over 30 dB. This discrepancy can be easily explained. Moving further away from the boundary, a collection of energy density sources can be viewed as a single source. Since a single energy source will transmit energy equally in all directions, a collection of energy sources will tend to transmit energy equally in all directions the further one moves from the boundary. Thus, for this directional case with one side pulsating, the ESSM could not model the physics of the real problem.

However, it is interesting to note that the ESSM could be carried out on only a portion of the boundary in close proximity to the field point region. Fig. 12 shows the set-up for such a case.

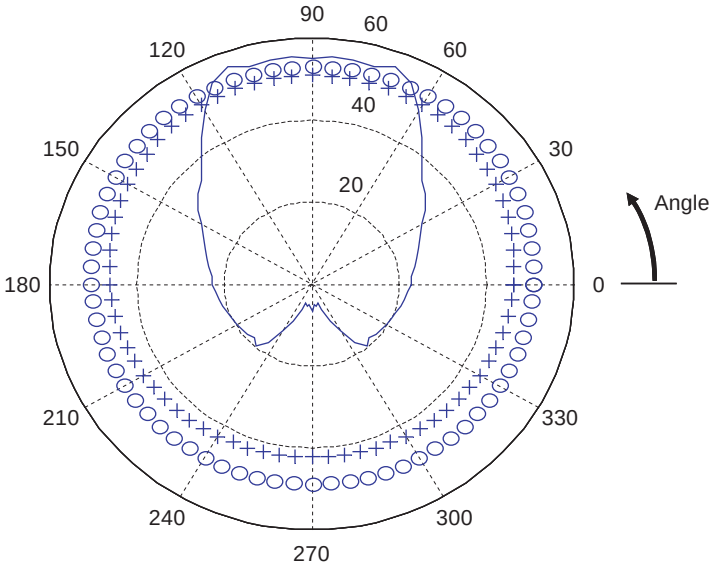

Fig. 11. ESSM energy density results for boundary condition Case C. The reference value for the energy density is 1.0e–12 J/m^3 (—, BEM energy density; + + +, ESSM energy density; ○, ESSM energy density obtained using the partial boundary shown in Fig. 12).

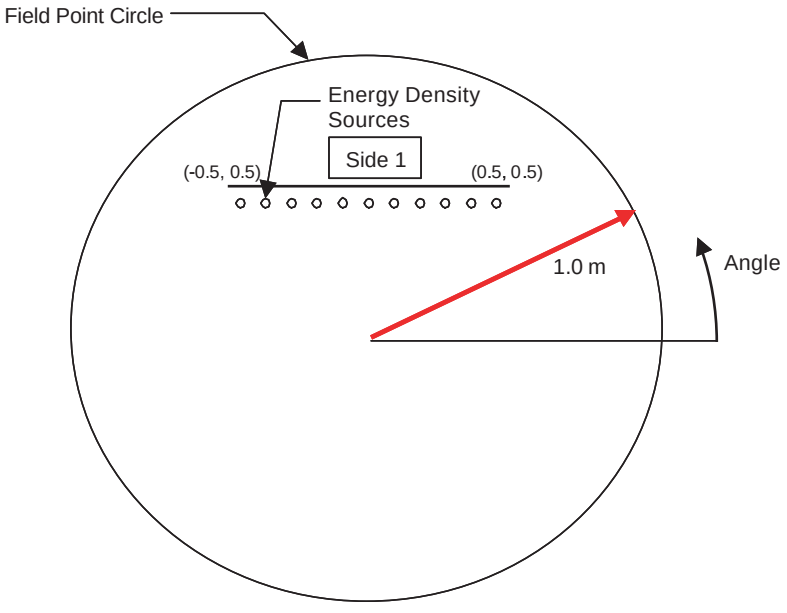

Fig. 12. Schematic showing the ESSM set-up assuming a partial boundary.

Notice that only the radiating side ($Y = 0.5$ m) is modeled. In this case, 11 energy density sources were placed below the boundary as indicated in the figure. The corresponding energy density results are also shown in Fig. 11. Notice that the maximum ESSM energy density (at the top of the

field point circle) was now only 2.3 dB less than the BEM energy density. However, the ESSM energy density results were in error by 4.3 dB if the entire boundary was modelled. Thus, the results suggest that the ESSM will more accurately predict the energy density if only the visible boundary elements from a field point are used. It is anticipated that the ESSM would have some advantages over SEA if only the visible elements to a field point were considered for a source solution.

5. Assessing the quality of the ESSM solution

The ESSM results were remarkably uniform regardless of the ESSM source locations. However, the question that naturally arises is how the user can determine the number and locations of virtual sources that will provide a satisfactory solution. This question was investigated by looking at a few quantities, which might give some indication of the goodness of the solution. These quantities include the radiated power, and the condition number of the $[B]$ matrix (Eq. (11)). The radiated power is equal to the integral of the intensity around the boundary. Thus, the radiated power can be calculated for both the normal intensity boundary condition and also for the normal intensity calculated from the sources. Specifically, the ESSM boundary condition and ESSM source generated radiated powers can be written as

$$\Pi_{B.C.} = \int_{\Gamma} I_n^{(B)} \mathrm{d}\Gamma \tag{16}$$

and

$$\Pi_{S.G.} = \int_{\Gamma} I_n^{(S.G.)} \mathrm{d}\Gamma, \tag{17}$$

respectively, where $I_n^{(B)}$ is the intensity boundary condition and $I_n^{(S.G.)}$ is the source generated intensity along the boundary.

The radiated sound power results are summarized in Table 1 for each of the seven source configurations. Fig. 6 shows Configuration A, and Fig. 13 shows Configurations B–G. All four sides were assumed to have equal normal intensity. The energy density results were similar (within 0.5 dB) for Configurations A–F. However, the results were judged to be unacceptable for Configuration G exhibiting little similarity to the other results (Configurations A–F).

Table 1
Tabular summary of the output power and condition numbers for each source configuration

ESSM source configuration	Output power (W)	Condition number of $[B]$
A	8.20e−06	55
B	7.89e−06	1
C	7.68e−06	3
D	8.16e−06	1650
E	8.15e−06	2.84e+09
F	8.19e−06	1.71e+09
G	8.23e−06	1.66e+14
ESSM B.C.	8.23e−06	

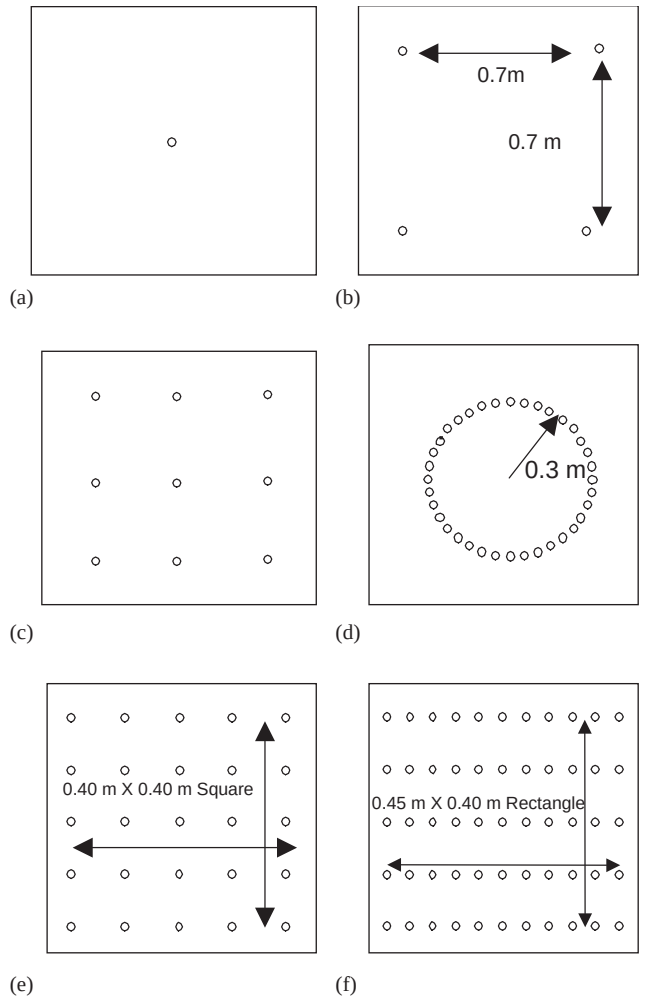

Fig. 13. Six additional source configurations. (a) Configuration B, (b) Configuration C, (c) Configuration D, (d) Configuration E, (e) Configuration F, and (f) Configuration G. Energy density sources are indicated by ○.

Notice that the source generated output power ($\Pi_{S.G.}$) compared well to the boundary condition radiated power ($\Pi_{B.C.}$) for each source configuration except for the single source configuration (Configuration B). Thus, comparing $\Pi_{S.G.}$ and $\Pi_{B.C.}$ des give some indication of the number of energy density sources that would be needed for an acceptable ESSM solution. In this example, it is apparent from sound power considerations that one energy density source is not enough. However, this comparison was not very indicative of the goodness of the ESSM solution. In fact, the output power for Configuration G (8.23e−6 W), a case where the ESSM solution was clearly unacceptable, was closest to the ESSM boundary condition radiated power (8.23e−6 W).

A better indicator of the goodness of the ESSM solution was the condition number of the [B] matrix. A matrix is considered ill conditioned if the condition number is too large (if the reciprocal of the condition number approaches the floating-point precision of the machine). Notice that the condition numbers for Configurations E–G (shown in Fig. 9) were on the order of 10^9 and 10^{14},

respectively, indicating that the ESSM solutions might be suspect. Using this criterion, Configuration A (shown in Fig. 6) appeared to be the best multi-source configuration. It should be noted that for each test case considered, the condition numbers were lower and the results compared best when the sources were located closer to the perimeter of the two-dimensional shape.

6. Test case 3—scattering examples

The ESSM was also applied to interior and exterior scattering cases. It should be noted before discussing the ESSM for interior cases, that the simplified energy method (SEM) might be a more appropriate method for looking at interior problems. In fact, Bouthier and Bernhard [4–6], Smith [8], and Palmer et al. [20] have successfully applied a SEM finite element code to membrane and plate problems that are analogous to the two-dimensional interior acoustics problem. However, the ESSM is considered for interior problems for the sake of completeness.

It was judged that plane wave energy density functions would be more appropriate than cylindrical energy density sources for interior problems. First of all, cylindrical energy density sources would have to be placed exterior to the boundary instead of inside the boundary. Since the domain exterior to the boundary is infinite, selecting source locations proved to be difficult. Secondly, a plane wave solution is, in fact, appropriate for some interior problems like the one-dimensional duct, and the rectangular waveguide [21]. Also, Bernhard et al. [4–6,12], Smith [8], and Palmer et al. [20] have successfully applied the SEM, which assumes a superposition of plane waves, to interior problems. The energy density function for a plane wave can be written as [3–6,8,14].

$$G(r_i) = \mathrm{e}^{-\eta k_0 r_i} \tag{18}$$

For the interior test case, a $1.0 \times 1.0\,\mathrm{m}^2$ geometry was again considered with a point source located within the square as indicated in Fig. 15. The fluid material properties in the interior were assumed to be those for air. Thus, the group speed and density were specified to be 343 m/s and $1.2\,\mathrm{kg/m}^3$, respectively. The boundary was assumed to be rigid. Thus, the normal velocity and intensity on the boundary were set to zero. Results were compared for a small dissipation constant of 0.01.

For the ESSM analysis, the boundary was discretized using 80 equal length elements around the perimeter. The ESSM analysis was conducted using plane wave functions arranged in the pattern shown in Fig. 14. As the figure indicates, the plane wave energy density functions were oriented 30° apart and centered at the center of the square.

A comparison between the BEM and the ESSM energy density results along the diagonal of the field point region is shown in Fig. 15. As the figure indicates, the ESSM results compared well to the BEM results suggesting that the ESSM could be reliably applied to simple interior scattering problems. Bouthier and Bernhard [4–6] noted similar results using the SEM for plates.

A similar exterior scattering analysis was conducted. A schematic showing the set-up is shown in Fig. 16. A point source was placed 0.5 m to the left of a rigid square boundary as indicated in Fig. 16. The boundary was 1.0 m × 1.0 m, and results were compared for a small dissipation factor of 0.01 again. Since this is an exterior example, cylindrical energy density sources were again used and arranged as indicated in Fig. 6. The analyses were again conducted over the 4000 Hz octave band.

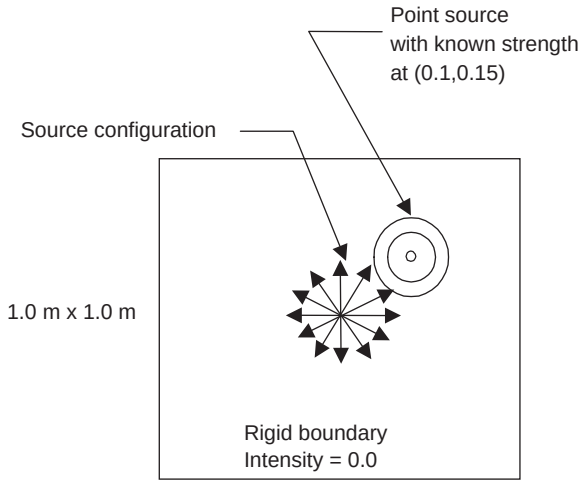

Fig. 14. Schematic showing the set-up for the interior scattering test case showing the location of the source and the source configuration. The origin is at the center.

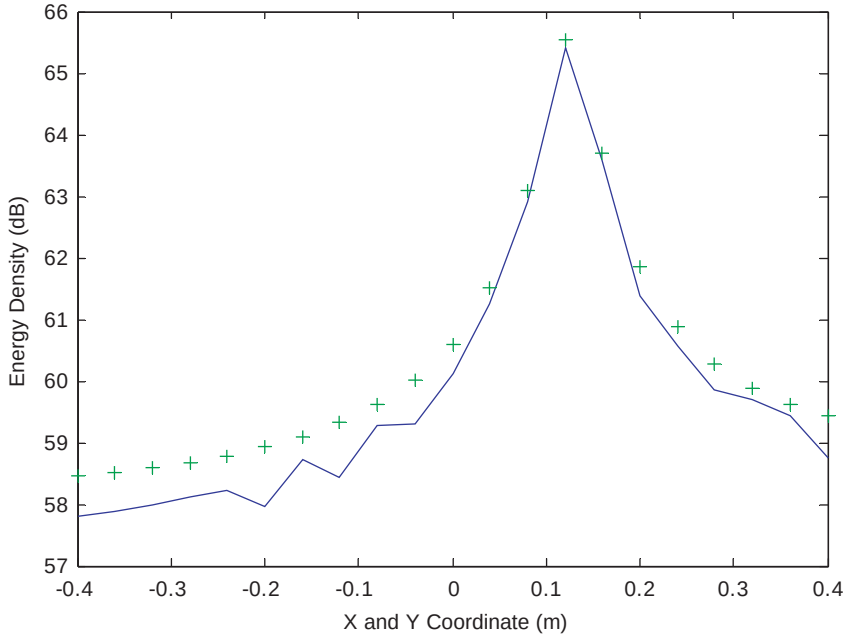

Fig. 15. Comparison of the BEM (—) to ESSM (+ + +) results along the diagonal of the square geometry. The reference energy density was 1.0e–12 J/m^3.

A comparison of the ESSM to the BEM results is shown in Fig. 17. The results compared well on the side closest to the point source. However, the ESSM over predicted the results on the side of the square opposite to the source by over 15 dB. The results demonstrate that

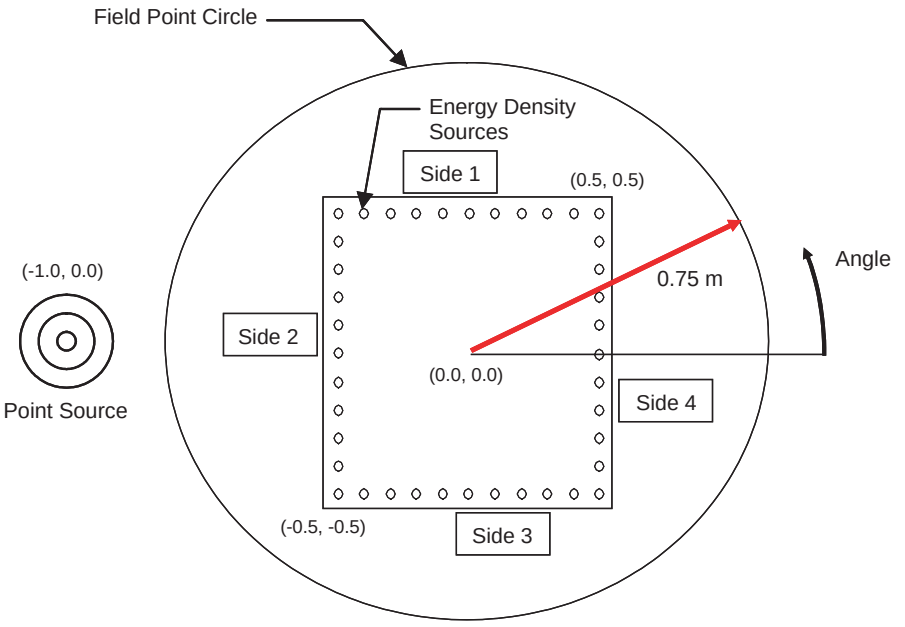

Fig. 16. Schematic showing the set-up for an exterior scattering test case. Energy density sources are indicated by ○.

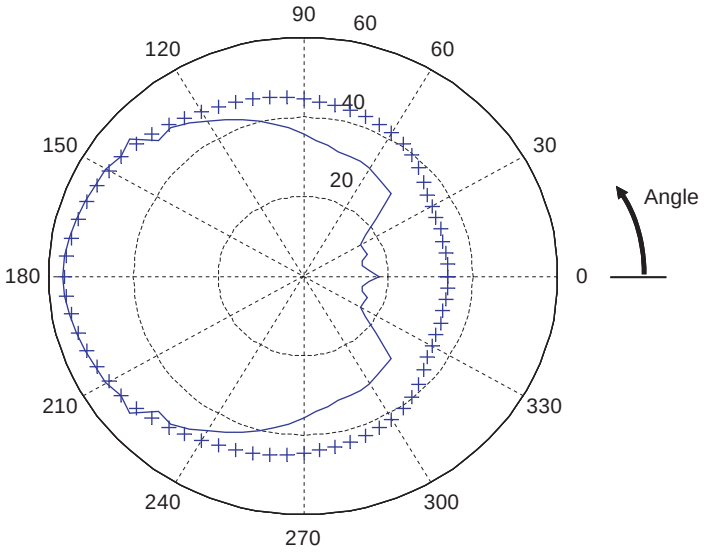

Fig. 17. ESSM energy density results for an exterior scattering case. The reference value for the energy density is 1.0e–12 J/m^3 (—, BEM energy density; + + +, ESSM energy density).

the ESSM cannot accurately calculate the actual directivity pattern. However, the ESSM did provide an excellent approximation of the energy density on the side closest to the point source.

7. Conclusion

In this paper, the ESSM was developed using an approach similar to the pressure source simulation approach [16,17]. However, energy density sources were used in the place of pressure sources. The method was validated using three different geometries. First, the ESSM energy density results were compared to the closed form results for a pulsating cylinder, and excellent agreement was noted. For the second set of test cases, a vibrating square was used. Due to the complexity of obtaining a closed form solution, the ESSM energy densities were compared to two-dimension BEM results. Again, the energy density results compared well if the results were averaged over a region of interest. However, it was noted that the ESSM did not perform as well for the directional case where only one side of the square vibrated. Finally, the ESSM was investigated for simple interior and exterior scattering test cases. A square geometry was again selected with a point source located on the interior or exterior. The results were especially promising for the interior case though there were some errors for the exterior example.

In conclusion, the results discussed suggest that the ESSM may be useful tool for analyzing high frequency acoustic problems. However, only a few test cases were performed, and more complex cases should be conducted to gage the usefulness of the method for more applied problems. Additionally, as the results for Case 2 indicate, the method is admittedly only a marginal improvement over SEA at this juncture. We believe that the method might be improved by adding additional source types. Currently, the point monopole energy source is the only source implemented in the ESSM. Additional energy sources could be developed (i.e., dipole energy sources) which may improve the results. Similar improvements were made to the multi-pole pressure source approach with good results [16].

It should also be noted that the ESSM requires a matrix to be computed and then for the unknown sources to be solved. Generally, these problems should be computationally small since the boundary mesh can be coarse, and the boundary condition is the spatially averaged normal intensity. As such, the ESSM is much faster than a conventional BEM analysis for a couple of reasons. First, the conventional BEM requires a certain number of elements per acoustic wavelength, and the size of the model necessarily increases along with the upper frequency limit. Secondly, results should be obtained for several frequencies in an octave band using the conventional BEM whereas one ESSM solution can be conducted at the center frequency of an octave band. Thus, the ESSM is a much faster high frequency approach than conventional BEM.

However, the ESSM cannot match the ease of use and speed of SEA. The main reasons being that the ESSM requires that a boundary mesh be created, and that matrices be synthesized and solved. On the other hand, SEA is a lumped parameter method and the size of the matrix depends chiefly on the number of subsystems in the SEA model.

Acknowledgements

The authors gratefully acknowledge the financial support provided by the University of Kentucky Center for Computational Sciences. Additionally, a special thanks is given to Dr. Robert Bernhard for his helpful advice and assistance.

References

[1] R.H. Lyon, R.G. DeJong, *Theory and Application of Statistical Energy Analysis*, 2nd Edition, Butterworth-Heinemann, Boston, MA, 1995.

[2] C.B. Burroughs, R.W. Fischer, F.R. Kern, An introduction to statistical energy analysis, *Journal of the Acoustical Society of America* 101 (1997) 1779–1789.

[3] D.J. Nefske, S.H. Sung, Power flow finite element analysis of dynamic systems: Basic theory and application to beams, statistical energy analysis: *Presented at the Winter Annual Meeting of American Society of Mechanical Engineers,* 1987, pp. 47–54.

[4] O.M. Bouthier, R.J. Bernhard, Models of space-averaged energetics of plates, *AIAA Journal* 30 (1992) 616–623.

[5] O.M. Bouthier, R.J. Bernhard, Simple models of the energy flow in vibrating membranes, *Journal of Sound and Vibration* 182 (1995) 129–147.

[6] O.M. Bouthier, R.J. Bernhard, Simple models of the energy flow of transversely vibrating plates, *Journal of Sound and Vibration* 182 (1995) 149–164.

[7] Y. Lase, M.N. Ichchou, L. Jezequel, Energy flow analysis of bars and beams: theoretical formulations, *Journal of Sound and Vibration* 192 (1996) 281–305.

[8] M.J. Smith, A hybrid energy method for predicting high frequency vibrational response of point-loaded plates, *Journal of Sound and Vibration* 202 (1997) 375–394.

[9] A. Le Bot, A vibroacoustic model for high frequency analysis, *Journal of Sound and Vibration* 211 (1998) 537–554.

[10] A. Le Bot, Geometric diffusion of vibrational energy and comparison with the vibrational conductivity approach, *Journal of Sound and Vibration* 212 (1998) 637–647.

[11] X. Zhao, N. Vlahopoulus, Coupling of finite element and energy finite element solutions for calculating the vibration of co-linear beams in the mid-frequency range, *SAE Noise and Vibration Conference & Exhibition*, Traverse City, MI, 1999, pp. 1091–1101.

[12] R.J. Bernhard, J.E. Huff, Structural-acoustic design at high frequency using the energy finite element method, *Proceedings of the 15th Biennial Conference on Vibration and Noise*, 1995, pp. 565–576.

[13] R.S. Langley, On the vibrational conductivity approach to high frequency dynamics for two-dimensional structural components, *Journal of Sound and Vibration* 182 (1995) 637–657.

[14] M.N. Ichchou, L. Jezequel, Comments on simple models of the energy flow in vibrating membranes and on simple models of the energetics of transversely vibrating plates, *Journal of Sound and Vibration* 195 (1996) 679–685.

[15] D.W. Herrin, A.F. Seybert, T.W. Wu, Energy source simulation method for solving two-dimensional acoustics problems, *Proceedings of the 137th Meeting of the Acoustical Society of America (on CD)*, Berlin, Germany, March 15–19, 1999.

[16] M. Ochmann, The source simulation technique for acoustic radiation problems, *Acustica* 81 (1995) 512–527.

[17] J.B. Fahnline, G.H. Koopmann, A numerical solution for the general radiation problem based on the combined methods of superposition and singular-value decomposition, *Journal of the Acoustical Society of America* 90 (1991) 2808–2819.

[18] F. Bitsie, The Structural-acoustic Energy Finite Element Method and Energy Boundary Element Method, Doctoral Dissertation, Purdue University. 1996.

[19] L. Cremer, M. Heckl, *Structure-Borne Sound*, 2nd Edition, Springer, Berlin, 1988.

[20] J.D. Palmer, E.J. Williams, C.H.J. Fox, Power flow in complex structures, *Proceedings for the 4th International Modal Analysis Conference*, Orlando, FL, 1993, pp. 115–121.

[21] L.E. Kinsler, A.R. Frey, A.B. Coppens, J.V. Sanders, *Fundamentals of Acoustics*, Wiley, New York, 1982.